Optical Coherence Tomography (OCT): A Review

Joseph M. Schmitt

(Invited Paper)

***Abstract*— This paper reviews the state of the art of optical coherence tomography (OCT), an interferometric imaging technique that provides cross-sectional views of the subsurface microstructure of biological tissue. Following a discussion of the basic theory of OCT, an overview of the issues involved in the design of the main components of OCT systems is presented. The review concludes by introducing new imaging modes being developed to extract additional diagnostic information.**

***Index Terms*— Imaging, interferometry, optical coherence tomography, speckle.**

I. Introduction

THE APPLICATION of optical technology in medicine and biology has a long and distinguished history. Since the 18th century, the microscope has been an indispensable tool of biologists. With the invention of the laser in the early 1960's, physicians gained a new surgical instrument. The development of fiber optics led to the manufacture of endoscopes that permit direct viewing of internal organs deep in the body. In the modern clinical laboratory, new optical technologies facilitate the chemical analysis of tissue samples and the counting and sizing of blood cells. In spite of these and other advances, few of the optical instruments used in medicine today take advantage of the coherent properties of light. Even most instruments that employ lasers, the ultimate generators of coherent light, can be classified as incoherent optical systems because the focused laser beam serves mainly as a source of illumination or concentrated heat. Perhaps one of the reasons why optical coherence tomography (OCT) has attracted the attention of engineers and scientists working in the photonics field is that it has the potential to become the first diagnostic imaging technology in which coherent optics features prominently.

OCT is a novel imaging technology that produces high-resolution cross-sectional images of the internal microstructure of living tissue [1]. Its first applications in medicine were reported less than a decade ago [1]–[5], but its roots lie in early work on white-light interferometry that led to the development of optical coherence-domain reflectometry (OCDR), a one-dimensional (1-D) optical ranging technique [6], [7]. Although OCDR was developed originally for finding faults in fiber-optic cables and network components, its ability to probe the eye [8]–[10] and other biological tissues [11], [12] was soon recognized. The superb optical sectioning ability of OCT, which is achieved by exploiting the short temporal coherence of a broadband light source, enables OCT scanners to image microscopic structures in tissue at depths beyond the reach of conventional bright-field and confocal microscopes. Probing depths exceeding 2 cm have been demonstrated in transparent tissues, including the eye and the frog embryo [13], [14]. In the skin and other highly scattering tissues, OCT can image small blood vessels and other structures as deep as 1–2 mm beneath the surface [4]–[16], [17]. An advantage that OCT has over high-frequency ultrasonic imaging, a competing technology that achieves greater probing depths but with lower resolution [18], is the relative simplicity and lower cost of the hardware on which OCT systems are based.

These attractive features notwithstanding, a number of technical problems must be overcome before OCT can take its place alongside the established diagnostic imaging modalities. Hidden behind the deceptive simplicity of the basic OCT system are complicated issues that relate to the generation and interference of partially coherent optical fields and how such fields propagate in biological tissue. Equally important are issues related to the design of practical interferometric scanning and detection systems. Rapid progress has been made over the last few years toward an understanding of these issues, which has led to new technologies for extending the capabilities of OCT. Keeping track of developments reported in journals and conferences that serve several diverse disciplines is becoming increasing difficult.

This review summarizes the technological advances in optical coherence tomography that have been made over the last ten years and places these advances in the context of key theoretical issues involved in imaging highly scattering tissue with partially coherent light. An overview of the technical issues involved in the design of the main components of an OCT system is presented. The review concludes with an introduction to parametric imaging modes of OCT that have been developed recently to acquire information about biological tissue in addition to its anatomical structure. Regrettably, a comprehensive summary of the technical issues of primary interest to optical engineers and scientists left little space for a discussion of the applications of OCT. Readers interested in this important topic should refer to earlier reviews by Fujimoto *et al.* [5], Izatt *et al.* [19], and Fercher [20].

Manuscript received October 26, 1998; revised June 1, 1999. This work was supported by the Hong Kong Research Grants Council under Grant HKUST 6002/97E.

J. M. Schmitt was with the Department of Electrical and Electronic Engineering, The Hong Kong University of Science and Technology, Clear Water Bay, Hong Kong. He is now with Mallinckrodt Corporation, Pleasanton, CA 94588 USA.

Publisher Item Identifier S 1077-260X(99)07521-8.

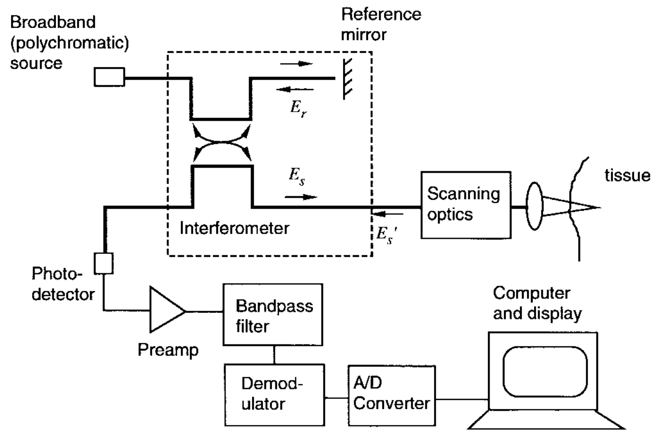

Fig. 1. Component blocks of an OCT system.

II. Theoretical Basis of OCT

Fig. 1 shows the basic components of an OCT system. At the heart of the system is an interferometer illuminated by a broadband light source. In this section the interferometer is first stripped to its bare essentials for analysis. Complications introduced by scattering in a tissue sample are introduced later in the section.

A. Low-Coherence Interferometry

The interferometer in an OCT scanner splits a broadband source field into a reference field E_r and sample field E_s. The sample field focuses through the scanning optics and objective lens to some point below the surface of the tissue. After scattering back from the tissue, the modified sample field E_s' mixes with E_r on the surface of the photodetector. Given the assumption that the photodetector captures all of the light from the reference and sample arms, the intensity that impinges on the photodetector is

$$I_d = \langle |E_d|^2 \rangle = 0.5(I_r + I_s') + Re\{\langle E_r^*(t+\tau)E_s'(t)\rangle\} \quad (1)$$

where I_r and I_s are the mean (dc) intensities returning from the reference and sample arms of the interferometer. The second term in this equation, which depends on the optical time delay τ set by the position of the reference mirror, represents the amplitude of the interference fringes that carry information about the tissue structure. The nature of the interference fringes—or whether any fringes form at all—depends on the degree to which the temporal and spatial characteristics of E_s' and E_r match. Thus the interferometer functions as a cross correlator and the amplitude of the interference signal generated after integration on the surface of the detector provides a measure of the cross-correlation amplitude. To facilitate the separation of the cross-correlation signal from the dc component of the intensity, various techniques have been devised to modulate τ. A few of these techniques are discussed in Section III-C.

Under the assumption that the tissue behaves as an ideal mirror that leaves the sample beam unaltered, the correlation amplitude depends on the temporal-coherence characteristics of the source, according to

$$Re[\langle E_s^*(t+\tau)E_s'(t)\rangle] = |G(\tau)| \cos[2\pi\nu_0\tau + \phi(\tau)] \quad (2)$$

where c is the speed of light, $\nu_0 = c/\lambda_0$ is the center frequency of the source, and $G(\tau)$ is its complex temporal-coherence function with argument $\phi(\tau)$. According to the Wiener–Khinchin theorem, $G(\tau)$ is related to the power spectral density of the source, $S(\nu)$, as [21]

$$G(\tau) = \int_0^\infty S(\nu)\ \exp(-j2\pi\tau)\ d\nu. \quad (3)$$

It follows from this relationship that the shape and width of the emission spectrum of the light source are important variables in OCT because of their influence on the sensitivity of the interferometer to the optical path difference. Section III-A discusses the properties of broadband sources that are suitable for use in OCT. Sources with broad spectra are desirable because they produce interference patterns of short temporal (and spatial) extent. The relationship between $S(\nu)$ and $G(\tau)$ can be seen clearly when both are represented by Gaussian functions:

$$S(\nu) \longleftrightarrow G(\tau) \quad (4)$$

with

$$S(\nu) = \frac{2\sqrt{\ln 2/\pi}}{\Delta\nu}\ \exp\left[-4\ \ln\ 2\left(\frac{\nu-\nu_0}{\Delta\nu}\right)^2\right] \quad (5)$$

and

$$G(\tau) = \exp\left[-\left(\frac{\pi\Delta\nu\tau}{2\sqrt{\ln\ 2}}\right)^2\right]\ \exp(-j2\pi\nu_0\tau). \quad (6)$$

In these equations, the half-power bandwidth $\Delta\nu$ represents the spectral width of the source in the optical frequency domain. The corresponding measure of the correlation width, derived from (6), is the (free-space) correlation length, given by

$$l_c = \frac{2c\ \ln(2)}{\pi} \cdot \frac{1}{\Delta\nu} \quad (7)$$

$$\approx 0.44\ \frac{\lambda_0^2}{\Delta\lambda} \quad (8)$$

where $\Delta\lambda$ is the full-width of the coherence function at half-maximum measured in wavelength units. Other definitions of the coherence length yield similar expressions, but with a different constant prefactors. For example, defined as the speed of light in the medium times the area under the squared amplitude of the normalized temporal coherence function, $l_c = c(\sqrt{2\ \ln(2)/\pi})/\Delta\nu \approx 0.66\lambda_0^2/\Delta\lambda$ [21]. In the OCT literature, (8) is the most common definition.

B. Tissue Scattering Models

In the derivation of the preceding expressions, the tissue was treated as an ideal mirror or coherent reflector. Propagation into the tissue and back was assumed to introduce a time delay, but otherwise leave the amplitude and coherence of the sample beam unchanged. Generally speaking, this is an unrealistic assumption. However, models based on a modified version of this assumption provide a satisfactory description of OCT imaging in the eye and other transparent tissues composed of weakly reflecting layers that are flat over the cross section of the sample beam [22]–[25]. In this special case, the interference signal can be expressed as a convolution,

$$I_s(\tau) = \sqrt{I_s' I_r}\sqrt{R(L_s)} \otimes |G(\tau)| \ \cos[2\pi\nu_0\tau] \qquad (9)$$

where $R(L_s)$ represents the fraction of power reflected from a layer located at position L_s in the tissue; the time delay of reflected sample beam relative to the reference beam is defined as $\tau = (L_s - L_r)/c$, with the position of the reference mirror given by L_r. This simple convolution model has been used in several studies [9], [12], [26], [27] to measure the locations and reflectivities of tissue layers in a manner analogous to pulse-echo ultrasound, with $|I_s(\tau)|^2$ interpreted as a reflectivity profile analogous to an A-mode ultrasound scan. It follows from (9) that the spatial extent of $|G(\tau)|$ determines the axial width of the point-spread function; therefore, in this one-dimensional model the coherence length is an appropriate measure of the axial resolution of the OCT system.

In the more general situation in which a two-dimensional cross-sectional image is built up from multiple axial scans, the optical transfer function of the optics that scan the beam and focus it into the tissue must be considered. Kempe and Rudolph [28] give expressions for the coherent point-spread function of interference microscopes in the single-scattering regime that are applicable to OCT imaging systems. They point out the equivalence between the imaging characteristics of confocal and interferometric systems in the transverse dimension and show that the temporal coherence of the light source does not influence the transverse point-spread function of microscope significantly for coherence times greater than about 20 fs. That is, except when the bandwidth of the source is very broad, the axial and transverse responses of the OCT system can be treated separately. Their studies also emphasize the impact of aberrations caused by focusing deep into a tissue through the air-tissue interface. Methods for correcting these aberrations, which become more severe as the numerical aperture (NA) of the objective lens increases, have been proposed for microscopes with a fixed focus [29], [30], but no practical method has yet been found for correcting aberrations dynamically in OCT systems that require focus to be maintained over a range of depths.

Although treating biological tissue as a collection of flat specular reflectors is convenient for theoretical analysis, the fact remains that most tissues are optically dense and do not conform well to this model. Soft tissue consists of a gelatinous matrix of collagen and elastin fibers packed with cells, blood vessels, nerves, and numerous other structures. The dimensions of the constituents of tissue range from less than 100 nm to more than several millimeters. When light is focused into tissue, the inhomogeneities in the refractive index cause the light to scatter at various angles [3], [31]. Fig. 2 categorizes the main types of scattering interactions. In the context of the present analysis, a fundamental questions arises: How do these scattering interactions affect the spatial and temporal coherence of returning sample beam? Several research groups

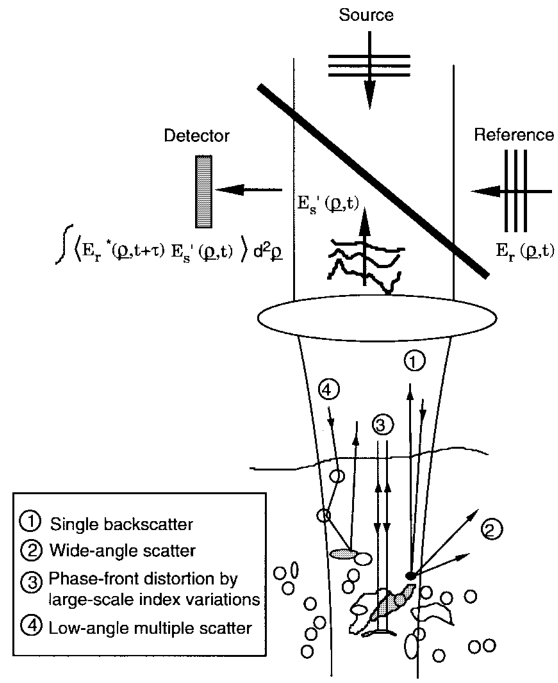

Fig. 2. Scattering interactions in tissue classified into four types (see inset). The reference field $E_r(\boldsymbol{\rho}, t)$ interferes with the distorted sample field $E_s'(\boldsymbol{\rho}, t)$ on the surface of the detector. The temporal cross-correlation product of the fields is integrated over the spatial domain $d^2\boldsymbol{\rho}$ defined by the area and collection angle of the detector. (Adapted from [3]).

have been working toward an answer to this question, which is central to the development of a comprehensive theory of optical coherence tomography [3], [32]–[36].

The basic aspects of attenuation of a focused beam in tissue composed of particulate scatterers are described by the single-backscattering model [37], which has been adapted to the analysis of OCT [32], [38]. This model, however, accounts for only the subset of possible scattering interactions that cause either total loss of coherence or no loss at all (those labeled "1" and "2" in Fig. 2). An article by Pan *et al.* [25] presents a linear systems model augmented by Monte Carlo simulations that takes a step closer to reality. It describes the loss of the coherence of the sample beam in terms of a convolution of the temporal coherence function of the OCT light source and the time-resolved reflectance function of the tissue. This article and another by Hellmuth [24] introduce the concept that OCT imaging systems respond to the discontinuities of the refractive index structure on the scale of a single wavelength. In effect, the coherence gate of an OCT system behaves as an optical bandpass filter centered on at $2\pi/\lambda_0$, with a width set by the coherence length of the source.

None of these models, however, accounts explicitly for the two-dimensional (2-D) spatiotemporal distribution of the backscattered field. Consequently, they give little insight into the degradation of imaging quality that results from the multiple scattering effects. Although the importance of multiple scattering has been confirmed by several experimental studies carried out on tissue phantoms [33], [39], [40], an effective measure that quantifies loss of contrast and resolution in images of real tissue has not yet been found. To aid quantification of these effects, Lindmo *et al.* [41]

developed a Monte Carlo simulation method that permits direct visualization of the loss of focus that results from multiple scattering. An analytical model developed by Schmitt and Knüttel [36] formulates the mutual-coherence function of the field backscattered from heterogeous tissue as a sum of the single- and multiple-forward-scattering contributions. Among the main findings that were obtained by applying this model to a fractal description of the size distribution of scatterers in tissue are: 1) low-angle multiple forward scattered light that passes through the temporal coherence gate degrades resolution and contrast, whereas light scattered at wide angles degrades contrast without affecting resolution significantly; 2) the maximum probing depth $z_{\max}$ in tissue is limited by the single-scattering coefficient and the mean scattering angle of the tissue. Estimates of these variables for skin and other highly scattering tissues yield $z_{\max} \sim 1.0$–1.5 mm (5–8 mean-free scattering lengths) at a wavelength of 1300 nm, a range that overlaps values estimated in other studies [28]; and 3) The coherence time of the source has a strong influence on the resolution of an OCT scanner because it determines the width of the axial point-spread function as well as the fineness of the speckle generated by multiple scattering.

C. Coherent Noise (Speckle)

Although many investigators have observed the effects of speckle on OCT imaging, its origins are not yet understood and only a few studies concerned with speckle reduction in OCT have been reported [42]–[44], [46]. Fig. 3(a) is an example of an OCT image of the skin in which the image-degrading effects of speckle are apparent. Most models of OCT wash away speckle by averaging the spatial properties of the tissue in the computation of the interference signal. Such averaging is not possible in practice because static tissue produces a stationary speckle pattern. There is a close connection between speckle generation and the optical bandpass response of OCT imaging systems, which makes the signal-carrying and signal-degrading roles of speckle hard to distinguish [46].

Ways of reducing the deleterious effects of speckle on OCT imaging include polarization diversity, frequency diversity, spatial diversity, and image postprocessing [47]. Most of these techniques trade resolution for reduction of speckle contrast. Effective speckle reduction requires widening the optical-frequency and spatial-frequency passbands of the OCT imaging system, which are limited by the source bandwidth and NA of the objective, respectively.

The OCT image in Fig. 3(b) illustrates the extent of speckle reduction that can be achieved by applying the spatial-diversity technique, while at the same time widening the source bandwidth and NA to compensate resolution losses. Features in Fig. 3(a) are much easier to resolve than those in Fig. 3(b), because the speckle in this image has a finer grain size and lower contrast.

Relatively little effort has been devoted to digital processing of OCT images for speckle reduction. Xiang *et al.* applied wavelet filters that incorporate automatic noise thresholds in an attempt to reduce high-frequency speckle noise without blurring edges [43]. Yung *et al.* showed that envelope distortion caused by coherent interference noise can be corrected by processing interference signals in the complex domain [44]. However, this technique appears to work effectively only when the number of scatterers in the sample volume is small. Although not designed specifically to reduce speckle noise, deconvolution methods developed by Kulkarni *et al.* [27] and Schmitt [45] reduce the effects of sidelobe interference which also contributes to coherent noise in OCT images.

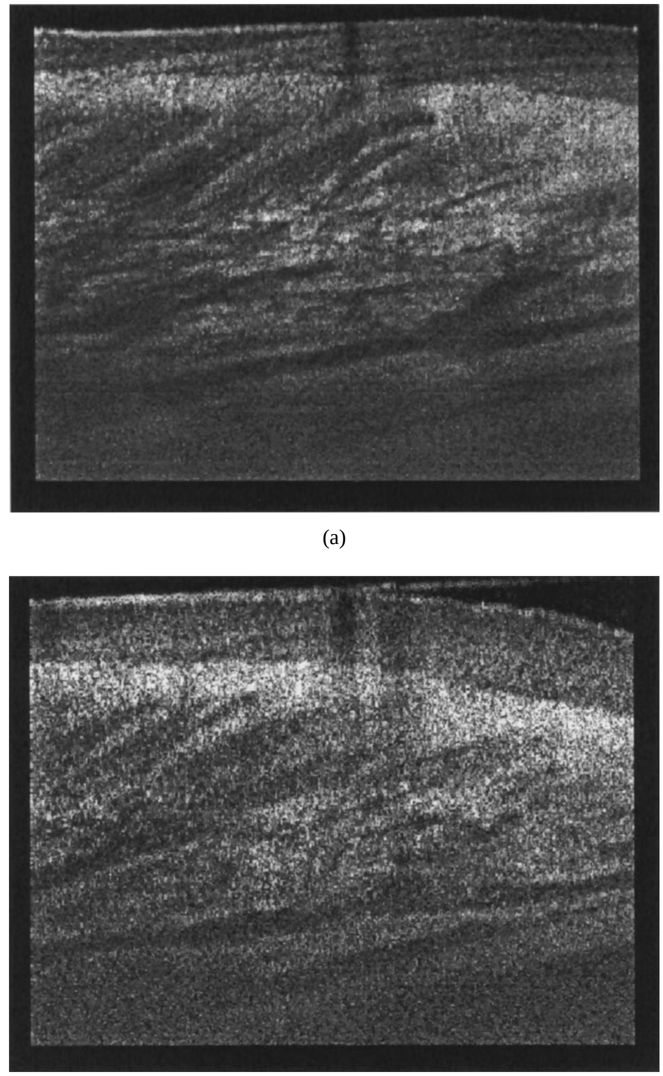

(a)

(b)

Fig. 3. Example of the effectiveness of speckle noise reduction achieved by spatial diversity processing in combination with source bandwidth broadening. (a) Image of skin formed from the incoherent sum of the envelopes of interference signals produced by four NA $= 0.2$ detectors and two sources (source bandwidth $\Delta\lambda = 80$ nm for $\lambda_0 = 1280$ nm). (b) Image of the same region of skin formed from the envelope of the interference signal produced by a single NA $= 0.4$ detector and a single source (source bandwidth $\Delta\lambda = 45$ nm for $\lambda_0 = 1300$ nm). Details of the apparatus and procedures used to obtain these images can be found in [52].

III. Hardware

This section presents an overview of the issues involved in the design of the optical components of the OCT system (Fig. 1). Since most of the technology employed in OCT is borrowed from the optical communications, it is not surprising that developments in this field have quickly become incorporated into OCT systems. The design of the hardware of OCT scanners is far from mature; therefore, this section provides only a snapshot of progress in this area.

A. Light Source

The results of several theoretical and experimental studies cited in Section II underscore the influence of the light source on the performance of the OCT system. The general requirements of sources for OCT imaging are: 1) emission in the near infrared; 2) short temporal coherence length; and 3) high irradiance.

The first requirement, emission in the near infrared, stems from the need to operate in a spectral range in which the penetration of light into tissue is adequate. Because of the short mean scattering length of photons in tissue at wavelengths in the blue and ultraviolet, OCT imaging with a source that emits in these spectral regions would be limited to superficial layers less than a few hundred micrometers thick. At wavelengths greater than 2500 nm, vibrational absorption by water limits imaging to similar depths. In studies carried out to date, the deepest penetration has been achieved using sources that emit at wavelengths between 1200 and 1800 nm [5], [48]. The optimum source wavelength for a given application may not be determined entirely by penetration depth. In particular, backscatter contrast and optical absorption (see Section IV-C) are wavelength-dependent variables that may also play a role in determining the contrast of OCT images.

The basis for the second requirement, short coherence length, is the relationship between the temporal coherence function of the light source and the width of the axial point-spread function of an OCT scanner (9). In general, the broader the emission bandwidth of the source, the better the resolution and contrast that can be achieved. However, to achieve the benefits of broadband operation of an OCT scanner, care must be taken to compensate for mismatches between the optical dispersion of the reference and sample beams [49] and the chromatic aberration of the focused beam caused by scattering in the tissue [39]. Also, the shape of the spectrum of the source is an important variable because it affects the dynamic range of the scanner near strong reflections [50].

The third requirement, high irradiance, is based on the need for wide dynamic range and high detection sensitivity for imaging weakly backscattering structures deep in tissue. Fortunately, because the interference signal is proportional to the square root of the power reflected from the target (9), a dynamic range exceeding 90 dB is not difficult to attain with a source power greater than a few hundred microwatts. The signal-to-noise ratio (SNR) of an interferometric imaging system is proportional to the source power concentrated in a single mode, which is limited by the requirement that the product of the diameter D of the source and its half-angle of emission α be of the order of a wavelength or less [51]

$$D\alpha \leq \lambda_0. \tag{10}$$

This requirement is even more stringent for wideband sources. Therefore, the most effective sources for OCT imaging emit light from a small spot over a wide angle or from a large spot over a narrow angle.

TABLE I
SHORT-COHERENCE SOURCES SUITABLE FOR USE IN OCT SYSTEMS

Source	Center wavelength (nm)	Bandwidth (nm)	Emission power	Reference
Edge-emitting LED	1300, 1550	50 - 100	20 - 300 μW	Derickson *et al* [99]
Superluminescent diode (SLD)	800 1300	20-30 40-50	1- 10 mW 1 - 5 mW	---- ----
Multiple QW LED/SLD	800 1480	90 90	15 mW max. 5 mW max.	Lin and Lee [53] Poole *et al* [54]
Laser-pumped fluorescent organic dye	590	40	9 mW	Liu *et al* [100]
Mode-locked $Ti:Al_2O_3$ laser	820	50-145	400 mW	Bouma *et al* [55]
Mode-locked Cr^{4+}:forsterite laser	1280	75	30 mW	Tearney *et al* [56]
Superfluorescent optical fibers:				
> Er-doped	1550	40 - 80	10 - 100 mW	Bouma *et al* [48]
> Tm-doped	1800	80	7 mW	"
> Nd-/Yb-doped	1060	65	108 mW	Paschotta *et al* [57]

Table I lists characteristics of a variety of light sources suitable for use in OCT systems. The most commonly used sources are edge-emitting light-emitting diodes (ELED's) and superluminescent diodes (SLD's) with peak emission wavelengths in either the 800- or 1300-nm fiber-optic telecommunications bands. Because of their high irradiance and relatively low cost, superluminescent sources come close to being the ideal sources for OCT imaging. However, the coherence lengths of SLD's (typically 15–30 μm) are not short enough to achieve the resolution required for many medical applications. ELED's with coherence lengths half as long are available commercially at low cost, but their emission powers are smaller by an order of magnitude. One way to overcome the tradeoff between the source power and bandwidth is to synthesize a broadband source by combining the outputs of several SLD's with different center wavelengths [52]. Multiple quantum-well devices achieve this synthesis by coupling the output of several sources on a single substrate [53], [54].

The source power required to maintain a given SNR increases with scanning speed. To meet the demands of the latest generation of OCT systems with scan rates that approach the television video rate, mode-locked $Ti:Al_2O_3$ and Cr^{4+} : forsterite lasers have been employed [55], [56]. The high power and wide bandwidth of these lasers (Table I) make them attractive sources for fast, high-resolution OCT imaging. However, their lack of portability limits their use to specialized applications. The diode-pumped superfluorescent fiber source is a lower cost and more compact alternative that can achieve comparable powers at bandwidths up to 80 nm. Table I gives the characteristics of three types of doped fibers that emit at wavelengths between 1000 and 1900 nm. Wider band operation can be achieved by splicing fibers doped with different materials [57].

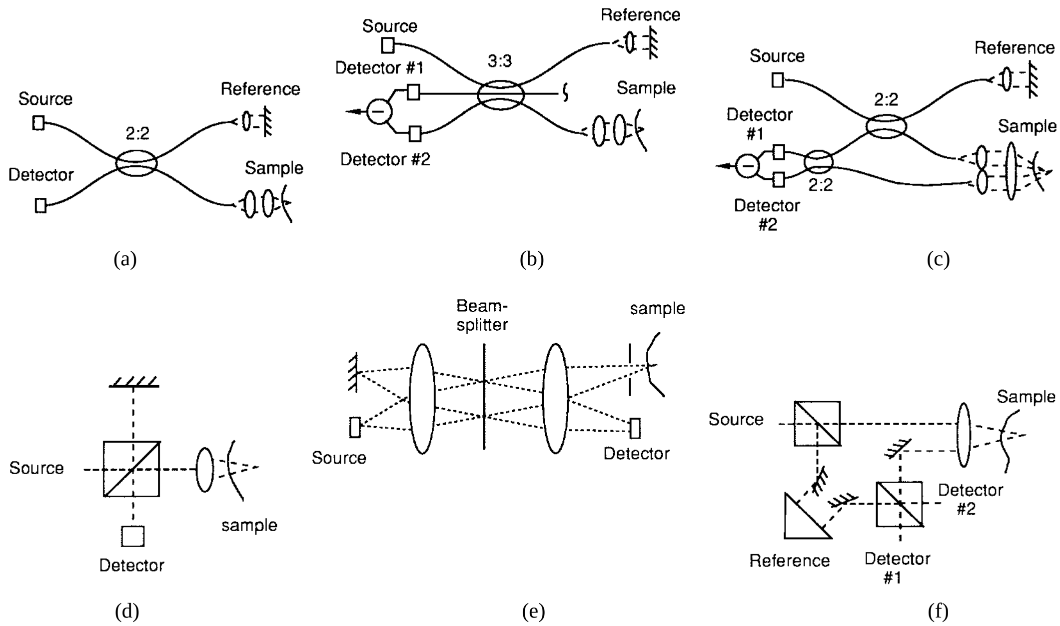

Fig. 4. Examples of interferometer configurations suitable for use in OCT systems. (a) Standard fiber-optic Michelson interferometer. (b) Balanced interferometer based on a 3 × 3 fiberoptic coupler [58]. (c) Balanced interferometer based on a pair of 2 × 2 fiberoptic couplers (An interferometer with a configuration similar to this was used in 98). (d) Free-space equivalent to the fiber-optic Michelson interferometer. (e) Compact in-line interferometer [59]. (f) Free-space Mach–Zehnder interferometer.

B. Interferometer

The most common interferometer configuration employed today in OCT systems is the fiber-optic Michelson interferometer illustrated in Fig. 4(a). In this type of interferometer, light from the source is conducted through a single-mode fiber to an evanescent-mode coupler where half of the optical power is extracted by another single-mode fiber that conducts the light to the reference mirror. The remaining half of the light enters the sample. The distal end of the fiber in the sample arm serves a dual role as a coherent light transceiver and spatial filter analogous to a confocal pinhole. A disadvantage of this configuration is that the dc signal and intensity noise generated by the light from the reference arm add to the interference signal. In balanced configurations, examples of which are shown in Figs. 4(b) and (c), these background noise components are cancelled by subtracting the photocurrents generated by two photodetectors (this subtraction can be done by placing the terminals of two photodiodes in opposition). The interference signals add at the output of the detectors because they vary out of phase [58]. The Mach–Zehnder configuration in Fig. 4(c) can be used either in the reflection or transmission modes.

The use of fiber optics is convenient, but not essential, in the design of OCT systems. In fact, in many applications free-space interferometers have distinct advantages. The availability of a wide variety of prisms and mirrors give the designer flexibility in layout of the interferometer, especially with respect to how light is coupled into and out of the reference and sample arms. Fig. 4(d)–(f) show a few of the many possible configurations of free-space interferometers suitable for use in OCT systems. The configuration in Fig. 4(d) is the equivalent of the fiber-optic Michelson interferometer, with the 2:2 fiber coupler replaced with a beamsplitter cube; Fig. 4(f) is the equivalent of the fiber-optic Mach–Zehnder configuration. As Fig. 4(e) illustrates, free-space optics can be made compact for use with semiconductor sources and detectors in handheld scanners [59]. Reducing polarization and dispersion mismatches between the reference and sample arms is also made easier in free-space interferometers. Because most single-mode optical fibers are made of silica, a birefringent material, changes in the polarization of the beam can be induced by bending; in addition, OH absorption in the silica limits the dispersion-free spectral width. These complications can be avoided in free-space interferometers.

C. Beam Scanning Optics

A difficult technical problem in the design of OCT systems is how to scan optical pathlength in the reference arm of the interferometer rapidly and precisely. The pathlength must be varied over a distance large enough to cover the desired axial imaging range, which may be as large as a centimeter or more for ocular imaging and 2 mm for imaging skin and other optically dense tissue, and its positioning inaccuracy must be a fraction of the source coherence length.

Most OCT systems reported to date rely on mechanical scanning mechanisms. Fig. 5 illustrates the basic layout of a few popular scanning methods. The simplest is based on translation of a reference mirror mounted on a stage driven by a dc motor or voice coil. A constant velocity v is maintained in the middle of the scan range by feedback control. The constant-velocity movement of the reference mirror shifts the center frequency of the interference signal to the Doppler frequency $f_d = 2v/\lambda_0$, which facilitates removal of the dc background and low-frequency noise during demodulation. The maximum sustained scanning speed that can be achieved with this approach is about 40 mm/s at a repetition rate of 30

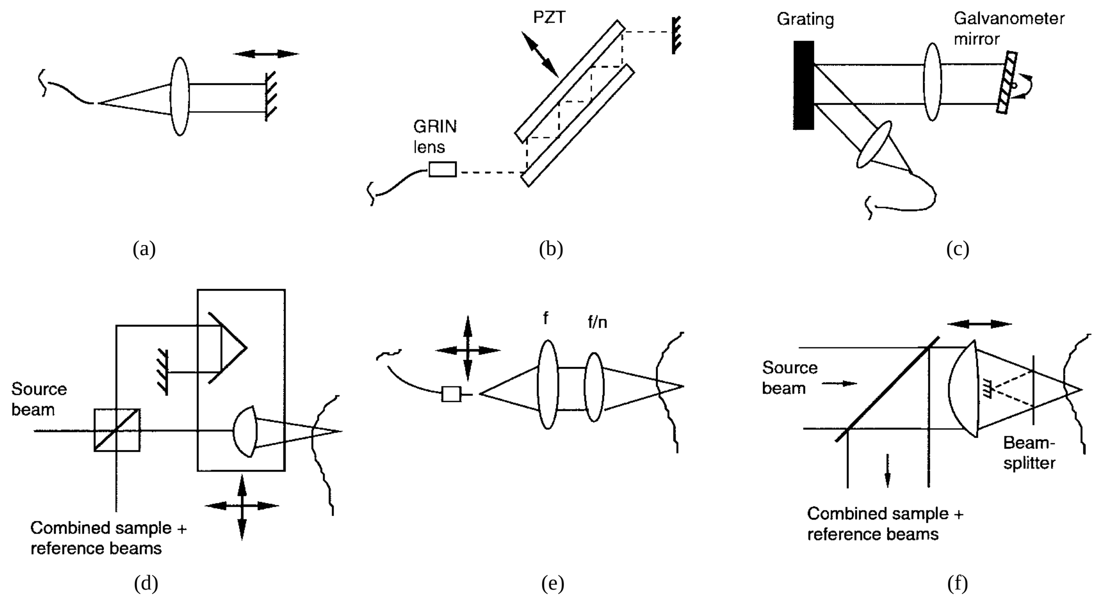

Fig. 5. Examples of techniques for scanning the reference pathlength in OCT systems. (a) Linear translating mirror. (b) Piezo-actuated optical delay-line constructed from parallel reflecting plates [30]. (c) FT optical delay line based on a lens-grating combination and an oscillating mirror [62]. (d) Free-space interferometer that uses a retroreflector in the reference arm and a moving objective to achieve dynamic focusing [52]. (e) Scanner that requires only movement of the tip of the sample fiber to achieve lateral and axial scanning, with the position of the reference mirror fixed [66], [67]. (f) Scanner based on the optical layout of a Mirau correlation microscope [68].

Hz. Comparable scanning speeds can be attained by using a piezoelectric transducer instead of a motor to drive a parallel mirror system in which light reflects multiple times [Fig. 5(b)] [17]. The development of faster mechanical scanning methods has been the subject of numerous recent studies [60]–[65]. To date, the fastest scan speeds and repetition rates (about 175 m/s at 25000 scans/s) have been achieved by an optical system based on a rotating beamsplitting cube driven by an air turbine [63]. The system illustrated in Fig. 5(c) can achieve scan rates almost as fast [64], [65] using readily available components. Designed originally for shaping femtosecond pulses, this system employs a grating-lens combination and an oscillating mirror to form an optical delay line [62].

All of the techniques discussed thus far provide a way to scan the reference pathlength, but fail to adjust the position of the objective lens in the sample arm to keep the focus on the optical path matchpoint. As a consequence, the axial scan range is limited to the Rayleigh range of the focused beam. Most researchers get around this problem by limiting the numerical aperture NA of the scanning optics to obtain a Rayleigh range of approximately 1 mm. At $\lambda = 1300$ nm, the corresponding focal spot diameter is about 30 μm for a Rayleigh range of this length. This spot size is too large for many high-resolution imaging applications. Several investigators have developed techniques that overcome this problem by scanning the reference pathlength and the position of the focused sample beam together [52], [59], [61], [66]. Fig. 5(d)–(f) show the optical layouts on which three such designs are based. Placing the reference mirror and objective lens on the same stage, as in the layout shown in Fig. 5(d), permits the use of a lens with an NA as large as 0.5 [52]. This layout provides for lateral and axial scanning of the beam and corrects the primary defocusing aberration caused by the refractive-index mismatch at the surface of the tissue. Designed for fiber-based OCT systems, the layout in Fig. 5(e) requires movement of the tip of the sample fiber only [66], [67]. It also provides for lateral and axial beam scanning and corrects the primary defocusing aberration. The layout shown in Fig. 5(f) is actually a self-contained interferometer based on the Mirau arrangement that can accommodate objectives with NA's as large as 0.8 [68]. Its drawbacks are that it does not correct defocus aberrations and special fabrication methods are required to make the miniature beamsplitter and mirror.

In an ideal OCT system, scanning of the reference pathlength and sample beam would require no moving parts at all. In principle, coherence tomography can be carried out by electronically recording the two-dimensional interference pattern formed at multiple optical delay times. This approach, which falls in the domain of 3-D electronic holography [69]–[71], has become an active area of OCT research [72]–[76]. An early report described a depth-profiling low-coherence reflectometer based on a stationary Fourier-transform spectrometer to which an acousto-optical scanner was later added to allow scanning in both the transverse and depth dimensions [72]. Fercher *et al.* [74] detailed the principles and application of spectral interferometry to the measurement of intraocular distances. In this technique, the single photodetector of the Michelson interferometer is replaced with a diode-array spectrometer that records a correlogram with the reference mirror fixed in position. Fourier transformation of the correlogram yields the reflectivity profile of the tissue in the depth dimension. More recently, Häusler and Lindner [76] developed a form of spectral interferometry called "spectral radar" that can be implemented simply by coupling a diode-array spectrometer to the output of a fiber-optic interferometer. They used such a system to obtain cross-sectional OCT images of the skin with a handheld scanner.

Present limitations of array detectors impose the main barriers to the development of no-moving-parts OCT scanners. Currently available 2-D arrays that operate at near-infrared wavelengths greater than 1000 nm are expensive and have relatively low dynamic ranges and readout rates. The use of a 1-D photodiode array with parallel readout for one scanning axis and a mechanical scanning apparatus for the other axis may provide a compromise solution.

IV. New Imaging Modes for Contrast Enhancement

As a noninvasive imaging method, optical coherence tomography must rely on the intrinsic variation of tissue properties to differentiate tissue constituents. In the majority of applications of OCT, the spatial variation of the coherent backscatter cross section is the primary source of contrast. In principle, however, any physical property that alters the amplitude, phase, or polarization of the sample beam can be used to extract information of diagnostic value. In this context, recent efforts have turned to exploring ways of exploiting new contrast mechanisms. In the last few years, four new OCT imaging modes have been demonstrated: 1) polarization; 2) Doppler; 3) absorption; and 4) elasticity. A brief review of each mode is given in the following paragraphs under separate headings.

A. Polarization

The electric fields that interfere to form the correlation signal measured in optical coherence tomography are actually vector quantities. For polarized sample and reference beams, the term in (1) that represents the fringe amplitude is the cross-correlation of the vector fields $\boldsymbol{E}_r = E_{x,r}\boldsymbol{x} + E_{y,r}\boldsymbol{y}$ and $\boldsymbol{E}'_s = E'_{x,s}\boldsymbol{x} + E'_{y,s}\boldsymbol{y}$. It follows that the interference signal measured by the low-coherence interferometer of an OCT system contains time (depth)-resolved information about the relative polarization states of the reference and sample beams.

Muscle, tendons, and other body tissues contain collagen and elastin fibers that exhibit birefringence when aligned in layers. Early in the development of OCT, polarization optics were added to the basic OCT system to permit depth-profiling of tissue birefringence [77]. The measurement of one-dimensional birefringence profiles was later extended to birefringence imaging of normal and thermally damaged soft tissue [78]–[80]. Further investigations using polarization-sensitive OCT revealed that the light backscattered from structures deep inside living skin is highly depolarized [81]. The depolarization was attributed to multiple scattering and to single-scattering from nonspherical particles [81].

The dependence of the Stokes parameters of a random media on the density, sizes, and arrangement of scatterers suggests that the full characterization of the polarization state of backscattered light may reveal information about tissue structure that is not apparent in OCT images obtained using randomly polarized light [82], [83]. Although the ability of polarization-sensitive OCT to enhance the contrast between healthy and pathological tissue has not yet been established in clinical trials, local changes in the the degree and state of polarization of the sample beam have been observed in laboratory studies of thermally damaged skin [80].

B. Doppler

For nearly two decades, laser Doppler velocimetry has been applied in a variety of medical studies, which include the measurement of blood flow in the skin, eye, and other organs [84], [85]. Because the laser has a long coherence length, interference between the static and Doppler-shifted components of the light scattered in tissue occurs over an extended optical path. Therefore, only coarse adjustment of the size and location of the sample volume probed by the velocimeter is possible via selection of the emission wavelength of the laser and the geometry of the probes.

The idea of employing coherence gating to define the sampling volume of a optical velocimeter was first applied to the measurement of flowing particles for the study of fluid mechanics [86]. Chen *et al.* took advantage of the coherence-gating ability of OCT to obtain images of the velocity profile of polystyrene beads in a tissue phantom [87] and blood flow in a rat skin model [88]. Izatt *et al.* pushed the technology of Doppler OCT further by developing methods to improve accuracy, speed, and sensitivity [89]–[91]. Boas [92] reported a novel method for measurement of the spatial variations in the Brownian motion of dense concentrations of scatterers with Doppler OCT.

Doppler OCT imaging has been demonstrated on tissue phantoms, embryos, and small animal skin-flap models [87], [88], [90]. Several technical challenges must be met before Doppler OCT can achieve sufficient accuracy over the range of depths required for imaging blood flow in human skin and other organs noninvasively. At present, the maximum probing depth of the OCT system limits imaging to blood vessels close to the surface of organs. Speckle noise modulates the spectrum of the backscattered signal, thereby reducing the signal-to-noise ratio of the centroid calculation from which estimates of the Doppler shift are derived [91]. Moreover, a tradeoff exists between the precision of velocity estimates and the image frame rate [91].

C. Absorption (Spectral)

The ability of OCT to measure the absorption spectrum of a sample can be seen by expressing the cross-correlation signal $I_c = Re[\langle E_r^*(t+\tau)E'_s(t)\rangle]$ in (1) as a product in the frequency domain [24], [94]

$$\tilde{I}_c(\nu) = \tilde{E}_r^*(\nu)\tilde{E}_s(\nu) \quad (11)$$

$$= \tilde{E}_r^*(\nu)\tilde{E}_r(\nu)|A(\nu)|\ \exp[-j\phi(\nu)] \quad (12)$$

$$= S(\nu)|A(\nu)|\ \exp[-j\phi(\nu)] \quad (13)$$

where $S(\nu)$ is the spectrum of the source and $A(\nu)$ and $\phi(\nu)$ are the amplitude and phase spectrum of the sample, respectively. Assuming that only single-scattering and absorption occur in the sample and that the real part of the refractive index changes negligibly over the range of optical depths 0 to $L = c\tau$, the amplitude spectrum and the absorption and scattering spectra at a given depth z' in the sample, $\mu_a(\nu, z')$

and $\mu_s(\nu, z')$, are related in the following way:

$$|A(\nu,L)|^2 \sim \mu_b(\nu,L) \cdot \exp\left[-2\int_0^L \mu_a(\nu,z') + \mu_s(\nu,z')dz'\right] \quad (14)$$

where $\mu_b(\nu, L)$ is the backscattering coefficient of the sample. For a uniformly absorbing and scattering sample in which scattering losses are negligible, this equation reduces to

$$|A(\nu,L)|^2 \sim \sigma_b(\nu)\ \exp[-2\mu_a(\nu)L] \quad (15)$$

from which an expression for the absorption spectrum is obtained,

$$\mu_a(\nu) \sim \frac{1}{2L}\ \ln\left(\frac{|A(\nu,0)|^2}{|A(\nu,L)|^2}\right) \quad (16)$$

$$\sim \frac{1}{2L}\ \ln\left(\frac{|\tilde{I}_c(\nu,0)/S(\nu)|^2}{|\tilde{I}_c(\nu,L)/S(\nu)|^2}\right). \quad (17)$$

Although the assumptions that lead to this result are unrealistic for highly scattering tissue samples at the wavelength of operation of current OCT systems, (17) embodies the basic mathematical operations that underlie spectral imaging with OCT. Provided that the influence of the scattering coefficients μ_b and μ_s can be eliminated, the absorption spectrum is proportional to the ratio of the logarithms of the normalized Fourier-transformed cross-correlation signals measured at two different depths in the medium. In principle, even the frequency dependence of the phase of the amplitude spectrum that results from optical dispersion in the sample can be extracted from the phase spectrum of the cross-correlation signal [94]. Quantitative measurement of local variations in tissue dispersion, especially in the eye, may have diagnostic value.

In a recent study, the feasibility of spectral imaging was demonstrated in tissue phantoms using an OCT system illuminated with two LED sources, one with its peak emission wavelength centered on a strong absorption band of water ($\lambda_1 = 1460$ nm) and the other with its peak emission outside this band ($\lambda_2 = 1300$ nm) [93]. To reduce the influence of scattering, the ratios of the logarithms of the squared correlation magnitudes at λ_1 and λ_2 were measured. However, because of the relatively low absorption losses relative to scattering losses at these wavelengths, the accuracy of the differential-absorption method still suffers from noise caused by speckle and spatial variations in the scattering coefficient.

As the compound in tissue with the strongest absorption in the near infrared, water is the natural compound to target for enhancing contrast in OCT imaging of biological tissue. Operation of an OCT system close to the edge of the strong OH absorption band centered on 1920 nm where the absorption and scattering coefficients of tissue are expected to have similar magnitudes may allow differentiation of tissue constituents on the basis of their fat, protein, and water contents. Spectral imaging OCT depends heavily on the characteristics of the source. Semiconductor diode sources that emit at wavelengths within strong water absorption bands are not available from commercial suppliers of fiberoptic components and must be custom manufactured. Laser-pumped superfluorescent fibers, such as the Tm-doped fiber (Table I), which emits close to the edge of the water absorption band that peaks at about 1920 nm, may be a suitable alternative to semiconductor diodes for absorption imaging.

D. Elasticity

The sensitivity of optical coherence tomography to displacement of living tissue during imaging is a troublesome problem that can lead to undesired blurring of images. OCT elastography takes advantage of this sensitivity to quantify microscopic deformations inside tissue induced by externally applied stress [95]. The goal of OCT elastography or elasticity imaging is to measure the local variations of the stiffness inside a tissue noninvasively. The primary quantitative measure of the stiffness is the shear elastic modulus, which varies widely for different types of tissue [96]. A number of disease processes, including edema, fibrosis, and calcification, alter the elastic modulus of the extracellular tissue matrix.

At the time of this review, only one exploratory study of OCT elastography has been carried out [95]. In this study, stress was applied to the tissue with a piezoelectric transducer attached to a glass plate through which the sample beam was focused. A sequence of A-line scans was taken in either the frame or line-by-line modes as the applied stress was increased. To generate cross-sectional images of the deformation and strain inside the tissue, the recorded interference signals were processed using computational methods borrowed from ultrasonic elastography. Using this procedure, deformation patterns in gelatin tissue phantoms, pork meat specimens, and intact skin were obtained with a resolution of a few micrometers.

Possible medical applications of OCT elastography include differentiation of hard and soft masses during tissue biopsy, imaging of arterial plaque composition, and evaluation of wound healing. OCT elastography may also aid efforts to solve fundamental problems in biomechanics, such as the role of microscopic deformations in the development of the embryo [97].

V. Concluding Remarks

Fueled by the explosion of innovations in the photonics field, the development of optical coherence tomography (OCT) has progressed rapidly over a period of less than 10 years. Whether this pace of development can be sustained and eventually lead to widespread use of OCT as a medical diagnostic technique depends on the ability of researchers to solve a number of tough problems that currently limit the performance of OCT systems. More powerful and broader band light sources, novel interferometer configurations, faster scanning techniques, and high-contrast imaging modes are a few of the ongoing developments that may lead to the solution of these problems. More effort is needed to put the theory of optical coherence tomography of biological tissue on a firmer foundation. As the history of other medical imaging modalities illustrates, the combination of solid theoretical analysis and new technology offers the best hope for success.

References

[1] D. Huang, E. A. Swanson, C. P. Lin, J. S. Schuman, W. G. Stinson, W. Chang, M. R. Hee, T. Flotte, K. Gregory, C. A. Puliafito, and J. G. Fujimoto, "Optical coherence tomography," *Science*, vol. 254, pp. 1178–1181, 1991.

[2] A. F. Fercher, C. K. Hitzenberger, W. Drexler, G. Kamp, and H. Sattmann, "In vivo optical coherence tomography," *Amer. J. Ophthalmol.*, vol. 116, pp. 113–114, 1993.

[3] J. M. Schmitt, A. Knüttel, M. Yadlowsky, and R. F. Bonner, "Optical-coherence tomography of a dense tissue: statistics of attenuation and backscattering" *Phys. Med. Biol.*, vol. 42, pp. 1427–1439, 1994.

[4] J. M. Schmitt, M. Yadlowsky, and R. F. Bonner, "Subsurface imaging if living skin with optical coherence tomography" *Dermatol.*, vol. 191, pp. 93–98, 1995.

[5] J. G. Fujimoto, M. E. Brezinski, G. J. Tearney, S. A. Boppart, B. E. Bouma, M. R. Hee, J. F. Southern, and E. A. Swanson, "Optical biopsy and imaging using optical coherence tomography," *Nature Med.*, vol. 1, pp. 970–972, 1995.

[6] R. C. Youngquist, S. Carr, and D. E. N. Davies, "Optical coherence-domain reflectometry: A new optical evaluation technique," *Opt. Lett.*, vol. 12, pp. 158–160, 1987.

[7] K. Takada, I. Yokohama, K. Chida, and J. Noda, "New measurement system for fault location in optical waveguide devices based on an interferometric technique," *Appl. Opt.*, vol. 26, pp. 1603–1606, 1987.

[8] A.F. Fercher, K. Mengedoht, and W. Werner, "Eye-length measurement by interferometry with partially coherent light," *Opt. Lett.*, vol. 13, pp. 1867–1869. 1988.

[9] C. K. Hitzenberger, W. Drexler, and A. F. Fercher, "Measurement of corneal thickness by laser doppler interferometry," *Invest. Ophthalmol. Vis. Sci.*, vol. 33, pp. 98–103, 1992.

[10] J. A. Izatt, M. R. Hee, E. A. Swanson, C. P. Lin, D. Huang, J. S. Schuman, C. A. Puliafito and J. G. Fujimoto, "Micrometer-scale resolution imaging of the anterior eye with optical coherence tomography," *Arch. Ophthalmol.*, vol. 112, pp. 1584–1589, 1994.

[11] W. Clivaz, F. Marquis-Weible, R. P. Salathe, R. P. Novak, and H. H. Gilgen, "High-resolution reflectometry in biological tissue," *Opt. Lett.*, vol. 17, pp. 4–6, 1992.

[12] J. M. Schmitt, A. Knüttel, and R. F. Bonner, "Measurement of optical properties of biological tissues by low-coherence reflectometry," *Appl. Opt.*, vol. 32, pp. 6032–6042, 1993.

[13] M. R. Hee, J. A. Izatt, E. A. Swanson, D. Huang, C. P. Lin, J. S. Schuman, C. A. Puliafito, and J. G. Fujimoto, "Optical coherence tomography of the human retina," *Arch. Ophthalmol.*, vol. 113, pp. 326–332, 1995.

[14] S. A. Boppart, M. E. Brezinsk, B. E. Boump, G. J. Tearney, and J. G. Fujimoto, "Investigation of developing embryonic morphology using optical coherence tomography," *Dev. Biol.*, vol. 177, pp. 54–64, 1996.

[15] J. Welzel, E. Lankenau, R. Birngruber, and R. Engelhardt, "Optical coherence tomography of the human skin," *J. Am. Acad. Derm.*, vol. 37, pp. 958–963, 1997.

[16] J. A. Izatt, M. D. Kulkarni, H. W. Wang, K. Kobayashi, and M. V. Sivak, "Optical coherence tomography and microscopy in gastrointestinal tissues," *IEEE J. Select. Topics Quantum Electron.*, vol. 2, pp. 1017–1028, 1996.

[17] Y. Pan, E. Lankenau, J. Welzel, R. Birngruber, and R. Engelhardt, "Optical coherence-gated imaging of biological tissues," *IEEE J. Select. Topics Quantum Electron.*, vol. 2, pp. 1029–1034, 1996.

[18] C. Passmann and H. Ermert, "A 100 MHz ultrasound imaging system for dermatologic and ophthalmologic diagnostics," *IEEE Trans. Ultrason., Ferroelect., Freq. Contr.*, vol. 43, pp. 545–552, 1996.

[19] J. A. Izatt, M. D. Kulkarni, K. Kobayashi, M. V. Sivak, J. K. Barton, and A. J. Welsh, "Optical coherence tomography for biodiagnostics," *Opt. Photon. News*, vol. 8, pp. 41–47, 1997.

[20] A. F. Fercher, "Optical coherence tomography," *J. Biomed. Opt*, vol. 1, pp. 157–173, 1996.

[21] J. W. Goodman, *Statistical Optics*. New York, NY: John Wiley and Sons: 1985, pp. 164–169.

[22] M. Davidson, K. Kaufman, I. Mazor, and F. Cohen, "An application of interference microscopy to integrated circuit inspection and metrology," *Proc. SPIE*, vol. 775, pp. 233–247, 1987.

[23] M. Kempe and W. Rudolph, "Scanning microscopy through thick layers based on linear correlation," *Opt. Lett.*, vol. 19, pp. 1919–1921, 1994.

[24] T. Hellmuth, "Contrast and resolution in optical coherence tomography," *Proc. SPIE*, vol. 2926, pp. 228–237, 1997.

[25] Y.T. Pan, R. Birngruber, J. Rosperich, and R. Engelhardt, "Low-coherence optical tomography in turbid tissue" *Appl. Opt.*, vol. 34, pp. 6564–6574, 1995.

[26] D. Huang, J. P. Wang, C. P. Lin, C. A. Puliafito, and J. G. Fujimoto, "Micron-resolution ranging of the cornea anterior chamber by optical reflectometry," *Lasers Surg. Med.*, vol. 11, pp. 419–425, 1991.

[27] M. D. Kulkarni, C. W. Thomas, and J. A. Izatt, "Image enhancement in optical coherence tomography using deconvolution," *Electron. Lett.*, vol. 33, pp. 1365–1367, 1997.

[28] M. Kempe and W. Rudolph, "Analysis of heterodyne and confocal microscopy for illumination with broad-bandwidth light," *J. Mod. Opt.*, vol. 43, pp. 2189–2204, 1996.

[29] C. J. R. Sheppard and C. J. Cogswell, "Effects of aberrating layers and tube length on confocal imaging properties," *Optik*, vol. 87, pp. 34–38, 1991.

[30] Z. Kam, D. A. Agard, and J. W. Sedat, "Three-dimensional microscopy in thick biological samples: A fresh approach for adjusting focus and correcting spherical aberration," *Bioimaging*, vol. 5, pp. 40–49, 1997.

[31] J. M. Schmitt and G. Kumar, "Turbulent nature of refractive index variations in biological tissue," *Opt. Lett.*, vol. 21, pp. 1310–1312, 1996.

[32] J. M. Schmitt, A. Knüttel, A. Gandjbakhche, and R. F. Bonner, "Optical characterization of dense tissues using low-coherence interferometry," *Proc. SPIE*, vol. 1889, pp. 197–211, 1993.

[33] M. J. Yadlowsky, J. M. Schmitt, and R. F. Bonner, "Multiple scattering in optical coherence tomography," *Appl. Opt.*, vol. 34, pp. 5699–5707, 1995.

[34] S. Q. Zeng, Q. M. Luo, X. D. Liu, Y. T. Pan, and Z. G. Li, "Analysis of two-dimensional image formation in optical coherence tomography," (in Chinese) *J. Infrared Millim. Waves*, vol. 14, pp. 429–434, 1995.

[35] Y. T. Pan, R. Birngruber, and R. Engelhardt, "Contrast limits of coherence-gated imaging in scattering media," *Appl. Opt.*, vol. 36, pp. 2979–2983, 1997.

[36] J. M. Schmitt and A. Knüttel, "Model of optical coherence tomography of heterogeneous tissue," *J. Opt. Soc. Amer. A*, vol. 14, 1231–1242, 1997.

[37] C. M. Sonnenschein and F. A. Horrigan, "Signal-to-noise relationships for coaxial backscatter from the atmosphere," *Appl. Opt.*, vol. 10, pp. 1600–1604, 1991.

[38] J. A. Izatt, M. R. Hee, G. M. Owen, E. A. Swanson, and J. G. Fujimoto, "Optical coherence microscopy in scattering media," *Opt. Lett.*, vol. 19, pp. 590–592, 1994.

[39] M. Kempe, A. Thon, and W. Rudolph, "Resolution limits of microscopy through scattering layers," *Opt. Commun.*, vol. 110, pp. 492–496, 1994.

[40] A. Knüttel, R. Schork, and D. Böcker, "Analytical modeling of spatial resolution curves in turbid media acquired with optical coherence tomography (OCT)," *Proc. SPIE*, vol. 2655, pp. 258–270, 1996.

[41] T. Lindmo, D. J. Smithies, Z. P. Chen, J. S. Nelson, and T. E. Milner, "Monte Carlo simulation studies of optical coherence tomography (OCT) and optical Doppler tomography (ODT)," *Proc. SPIE*, vol. 3251, pp. 114–125, 1998.

[42] J. M. Schmitt, "Array detection for speckle reduction in optical coherence microscopy," *Phys. Med. Biol.*, vol. 42, pp. 1427–1439, 1997.

[43] S. H. Xiang, L. Zhou, and J. M. Schmitt, "Speckle noise reduction for optical coherence tomography," *Proc. SPIE*, vol. 3196, pp. 79–88, 1997.

[44] K. M. Yung, J. M. Schmitt, and S. L. Lee, "Digital processing of noisy OCT signals in phase space," *Proc. SPIE*, vol. 3251, pp. 2–11, 1997.

[45] J. M. Schmitt, "Restoration of optical coherence images of living tissue using the CLEAN algorithm," *J. Biomed. Optics*, vol. 3, pp. 66–75, 1998.

[46] J. M. Schmitt, S. H. Xiang, and K. M. Yung, "Speckle in optical coherence tomography," *J. Biomed. Optics*, submitted.

[47] F. Forsberg, A. J. Healey, A. J. Leeman, and J. A. Jensen, "Assessment of hybrid speckle reduction algorithms," *Phys. Med. Biol.*, vol. 36, pp. 1539–1549, 1991.

[48] B. E. Bouma, L. E. Nelso, G. J. Tearney, D. J. Jones, M. E. Brezinski, and J. G. Fujimoto, "Optical coherence tomographic imaging of human tissue at 1.55 μm and 1.81 μm using Er- and Tm-doped fiber sources," *J. Biomed. Opt.*, vol. 3, pp. 76–79, 1998.

[49] C. K. Hitzenberger, A. Baumgartner, and A. F. Fercher, "Dispersion-induced multiple signal peak splitting in partial coherence interferometry," *Opt. Commun.*, vol. 154, pp. 179–185, 1998.

[50] S. R. Chinn and E. A. Swanson, "Blindness limitations in optical coherence domain reflectometry," *Electron. Lett.*, vol. 294, pp. 2025–2027, 1993.

[51] J. Y. Wang, "Detection efficiency of coherent optical radar," *Appl. Opt.*, vol. 23, pp. 3421–3427, 1984.

[52] J. M. Schmitt, S. L. Lee, and K. M. Yung, "An optical coherence microscope with enhanced resolving power," *Opt. Commun.*, vol. 142, pp. 203–207, 1997.

[53] C. F. Lin and B. L. Lee, "Extremely broadband AlGaAs/GaAs superluminescent diodes," *Appl. Phys. Lett.*, vol. 71, pp. 1598–1600, 1997.

[54] P. J. Poole, M. Davies, M. Dion, Y. Feng, S. Charbonneau, R. D. Goldberg, and I. V. Mitchell, "The fabrication of a broad-spectrum

light-emitting diode using high-energy ion implantation," *IEEE Photon. Technol. Lett.*, vol. 8, pp. 1145–1147, 1996.
[55] B. E. Bouma, G. J. Tearney, S. A. Boppart, M. R. Hee, M. E. Brezinski, and J. G. Fujimoto, "High-resolution optical coherence tomographic imaging using a mode-locked $Ti : Al_2O_3$ laser source," *Opt. Lett.*, vol. 20, pp. 1486–1488, 1995.
[56] G. J. Tearney, M. E. Brezinski, B. E. Bouma, S. A. Boppart, C. Pitris, J. F. Southern, and J. G. Fujimoto, "In vivo endoscopic optical biopsy with optical coherence tomography," *Science*, vol. 276, pp. 2037–2039, 1997.
[57] R. Paschotta, J. Nilsson, A. C. Tropper, and D. C. Hanna, "Efficient superfluorescent light sources with broad bandwidth," *IEEE J. Select. Topics Quantum Electron.*, vol. 3, pp. 1097–1099, 1997.
[58] K. Takada, H. Yamada, and M. Horiguchi, "Optical low coherence reflectometer using [3 × 3] fiber coupler," *IEEE Photon. Technol. Lett.*, vol. 6, pp. 1014–1016, 1994.
[59] J. M. Schmitt, "Compact in-line interferometer for low-coherence interferometry," *Opt. Lett.*, vol. 20, pp. 419–421, 1995.
[60] E. A. Swanson, D. Huang, M. R. Hee, J. G. Fujimoto, C. P. Lin, and C. A. Puliafito, "High-speed optical coherence domain reflectometry," *Opt. Lett.*, vol. 17, pp. 151–153, 1992.
[61] R. Windecker, M. Fleischer, B. Franze, and H. J. Tiziani, "Two methods for fast coherence tomography and topometry," *J. Mod. Opt.*, vol. 44, pp. 967–977, 1997.
[62] C. B. Su, "Achieving variation of the optical path length by a few millimeters at millisecond rates for imaging of turbid media and optical interferometry: A new technique," *Opt. Lett.*, vol. 22, pp. 665–667, 1997.
[63] J. Szydlo, N. Delachenal, R. Gianotti, R. Wälti, H. Bleuler, and R. P. Salathé, "Air-turbine driven optical low-coherence reflectometry at 28.6-kHz scan repetition rate," *Opt. Commun.*, vol. 154, pp. 1–4, 1998.
[64] G. J. Tearney, B. E. Bouma, and J. G. Fujimoto, "High speed phase- and group-delay scanning with a grating-based phase control delay line," *Opt. Lett.*, vol. 22, pp. 1811–1813, 1997.
[65] A. M. Rollins, M. D. Kulkarni, S. Yazdanfar, R. Ung-arunyawee, and J. A. Izatt, "In vivo video rate optical coherence tomography," *Opt. Express*, vol. 3, pp. 219–229, 1998.
[66] F. Lexer, A. F. Fercher, H. Sattmann, W. Drexler, and S. Molebny, "Dynamic coherent focus for transversal resolution enhancement," *Proc. SPIE*, vol. 3251, pp. 85–90, 1998.
[67] A. Knüttel, Boehringer-Mannheim Corporation, Mannheim, Germany, personal communication.
[68] G. S. Kino and S. S. C. Chim, "Mirau correlation microscope," *Appl. Opt.*, vol. 29, pp. 3775–3783, 1990.
[69] E. N. Leith, J. Upatnieks, and K. A. Haines, "Microscopy by wavefront reconstruction," *J. Opt. Soc. Am.*, vol. 55, pp. 981–986, 1965.
[70] K. G. Spears, J. Serafin, N. H. Abramson, X. M. Zhu, and H. Bjelkhagen, "Chrono-coherent imaging for medicine," *IEEE Trans. Biomed. Eng.*, vol. 36, pp. 1210–1221, 1989.
[71] E. N. Leith, C. Chen, H. Chen, Y. Chen, D. Dilworth, J. Lopez, J. Rudd, P.C. Sun, J. Valdmanis, and G. Vossler, "Imaging through scattering media with holography," *J. Opt. Soc. Amer. A*, vol. 9, pp. 1148–1153, 1992.
[72] A. Knüttel and J. M. Schmitt, "Stationary depth-profiling reflectometer based on low-coherence interferometry," *Opt. Commun.*, vol. 102, pp. 193–198, 1993.
[73] A. Knüttel, J. M. Schmitt, and J. R. Knutson, "Low-coherence reflectometry for stationary lateral and depth profiling with acousto-optic deflectors and a CCD camera," *Opt. Lett.*, vol. 19, pp. 302–304, 1994.
[74] A. F. Fercher, C. K. Hitzenberger, G. Kamp, and S. Y. El-Zaiat, "Measurement of intraocular distances by backscattering spectral interferometry," *Opt. Commun.*, vol. 117, pp. 43–48, 1995.
[75] R. Lazar, H. Brunner, and R. Steiner, "Optical coherence tomography (OCT) of human skin with a slow-scan CCD camera," *Proc. SPIE*, vol. 2925, pp. 143–151, 1996.
[76] G. Häusler and M. W. Lindner, "Coherence radar and spectral radar—new tools for dermatological diagnosis," *J. Biomed. Opt.*, vol. 3, pp. 21–31, 1998.
[77] M. R. Hee, D. Huang, E. A. Swanson, and J. G. Fujimoto, "Polarization-sensitive low-coherence reflectometer for birefringence characterization and ranging," *J. Opt. Soc. Am. A*, vol. 9, pp. 903–908, 1992.
[78] J. F. De Boer, T. E. Milner, M. J. C. van Gemert, and J. S. Nelson, "Two-dimensional birefringence imaging in biological tissue by polarization-sensitive optical coherence tomography," *Opt. Lett.*, vol. 22, pp. 934–936, 1997.
[79] M. J. Everett, K. Schoenenberger, B. W. Colston, Jr., and L. B. Da Silva, "Birefringence characterization of biological tissue by use of optical coherence tomography," *Opt. Lett*, vol. 23, pp. 228–230, 1998.
[80] J. F. De Boer, S. M. Srinivas, A. Malekafzali, and Z. P. Chen, and J. S. Nelson, "Imaging thermally damaged tissue by polarization sensitive optical coherence tomography," *Opt. Express*, vol. 3, pp. 212–218, 1998.
[81] J. M. Schmitt and S. H. Xiang, "Cross-polarized backscatter in optical coherence tomography of biological tissue," *Opt. Lett*, vol. 23, pp. 1060–1062, 1998.
[82] M. I. Mishchenko and J. W. Hovenier, "Depolarization of light backscattered by randomly oriented nonspherical particles," *Opt. Lett*, vol. 20, pp. 1356–1358, 1995.
[83] A. Ambirajan and D. C. Look, "A backward Monte Carlo study of the multiple scattering of a polarized laser beam," *J. Quantum Spectrosc. Radiat. Transfer*, vol. 58, pp. 171–192, 1997.
[84] M. D. Stern, "In vivo evaluation of microcirculation by coherent light scattering," *Nature*, vol. 254, pp. 56–58, 1975.
[85] T. Tanaka, C. Riva, and I. Ben-Sira, "Blood velocity measurements in human retinal vessels," *Science*, vol. 186, pp. 830–831, 1974.
[86] V. Gusmeroli and M. Martinelli, "Distributed laser Doppler velocimeter," *Opt. Lett*, vol. 16, pp. 1358–1360, 1991.
[87] Z. P. Chen, T. E. Milner, D. Dave, and J. S. Nelson, "Optical Doppler tomographic imaging of fluid flow velocity in highly scattering media," *Opt. Lett*, vol. 22, pp. 64–66, 1997.
[88] Z. P. Chen, T. E. Milner, S. Srinivas, X. J. Wang, A. Malekafzali, M. J. C. van Gemert, and J. S. Nelson, "Noninvasive imaging of in vivo blood flow velocity using optical Doppler tomography," *Opt. Lett*, vol. 22, pp. 1–3, 1997.
[89] J. A. Izatt, M. D. Kulkarni, S. Yazdanfar, J. K. Barton, and A. J. Welsh, "In vivo color Doppler imaging of picoliter blood volumes using optical coherence tomography," *Opt. Lett*, vol. 22, pp. 1439–1441, 1997.
[90] S. Yazdanfar, M. D. Kulkarni, and J. A. Izatt, "High-resolution of in-vivo cardiac dynamics using color Doppler optical coherence tomography," *Opt. Express*, vol. 1, pp. 424–431, 1997.
[91] M. D. Kulkarni, T. G. van Leeuwen, S. Yazdanfar, and J. A. Izatt, "Velocity-estimation accuracy and frame-rate limitations in color Doppler optical coherence tomography," *Opt. Lett.*, vol. 23, pp. 1057–1059, 1997.
[92] D. A. Boas, K. K. Bizheva, and A. M. Siegel, "Using dynamic low-coherence interferometry to image Brownian motion within highly scattering media," *Opt. Lett.*, vol. 23, pp. 319–321, 1998.
[93] J. M. Schmitt, S. H. Xiang, and K. M. Yung, "Differential absorption imaging with optical coherence tomography," *J. Opt. Soc. Amer. A*, vol. 15, pp. 2288–2296, 1998.
[94] T. Fuji, M. Miyata, S. Kawato, T. Hattori, and H. Nakatsuka, "Linear propagation of light investigated with a white-light interferometer," *J. Opt. Soc. Amer. B*, vol. 14, pp. 1074–1078, 1997.
[95] J. M. Schmitt, "OCT elastography: Imaging microscopic deformation and strain of tissue," *Opt. Express*, vol. 3, pp. 199–211, 1998.
[96] A. P. Sarvazyan, A. R. Skovoroda, S. Y. Emelianov, J. B. Fowlkes, J. G. Pipe, R. S. Adler, R. B. Buxton, and P. L. Carson, "Biophysical bases of elasticity imaging," *Acoust. Imaging*, vol. 21, pp. 223–240, 1995.
[97] R. Gordon, "A review of theories of vertebrate neurulation and their relationship to the mechanics of neural tube defects," *J. Embryol. Exp. Morph.*, vol. 89, pp. 229–255, 1985 (suppl.).
[98] M. R. Hee, J. A. Izatt, J. M. Jacobson, and J. G. Fujimoto, "Femtosecond transillumination optical coherence tomography," *Opt. Lett.*, vol. 18, pp. 950–952, 1993.
[99] D. J. Derickson, P. A. Beck, T. L. Bagwell, D. M. Braun, J. E. Fouquet, F. G. Kellert, M. J. Ludowise, W. H. Perez, T. R. Ranganath, G. R. Trott, and S. R. Sloan, "High-power, low-internal-reflection, edge emitting light-emitting diodes," *Hewlett-Packard J.*, vol. 46, pp. 43–49, 1995.
[100] H. H. Liu, P. H. Cheng, and J. P. Wang, "Spatially coherent white-light interferometer based on a point fluorescent source," *Opt. Lett.*, vol. 18, pp. 678–680, 1993.

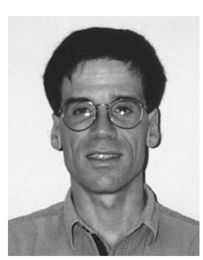

Joseph M. Schmitt received the B.S. degree in biomedical engineering from Case Western Reserve University, Cleveland, OH, in 1977 and the M.S. and Ph.D. degrees in electrical engineering from Stanford University, Stanford, CA, in 1981 and 1986, respectively.

He was an Associate Professor in the Department of Electrical Engineering and Co-Director of the Center for Medical Diagnostic Technology at the Hong Kong University of Science and Technology, Clear Water Bay, Hong Kong. In January 1999, he joined the Respiratory Division of Mallinckrodt Corporation, Pleasanton, CA.